Simple mechanism whereby the F_1-ATPase motor rotates with near-perfect chemomechanical energy conversion

Ei-ichiro Saita[a,b], Toshiharu Suzuki[a,b,c], Kazuhiko Kinosita Jr.[c], and Masasuke Yoshida[a,b,1]

[a]Department of Molecular Bioscience, Kyoto Sangyo University, Kamigamo Motoyama, Kyoto 603-8555, Japan; [b]International Cooperative Research Project, ATP Synthesis Regulation Project, Japan Science and Technology Agency, Aomi 2-3-6, Tokyo 135-0064, Japan; and [c]Department of Physics, Faculty of Science and Engineering, Waseda University, Shinjuku-ku, Tokyo 169-8555, Japan

Edited by Martin Karplus, Harvard University, Cambridge, MA, and approved June 23, 2015 (received for review December 1, 2014)

F_1-ATPase is a motor enzyme in which a central shaft γ subunit rotates 120° per ATP in the cylinder made of $\alpha_3\beta_3$ subunits. During rotation, the chemical energy of ATP hydrolysis (ΔG_{ATP}) is converted almost entirely into mechanical work by an elusive mechanism. We measured the force for rotation (torque) under various ΔG_{ATP} conditions as a function of rotation angles of the γ subunit with quasi-static, single-molecule manipulation and estimated mechanical work (torque × traveled angle) from the area of the function. The torque functions show three sawtooth-like repeats of a steep jump and linear descent in one catalytic turnover, indicating a simple physical model in which the motor is driven by three springs aligned along a 120° rotation angle. Although the second spring is unaffected by ΔG_{ATP}, activation of the first spring (timing of the torque jump) delays at low [ATP] (or high [ADP]) and activation of the third spring delays at high [P_i]. These shifts decrease the size and area of the sawtooth (magnitude of the work). Thus, F_1-ATPase responds to the change of ΔG_{ATP} by shifting the torque jump timing and uses ΔG_{ATP} for the mechanical work with near-perfect efficiency.

F_1-ATPase | rotary motor | single molecule | torque | ATP synthase

The F_oF_1-ATP synthase (F_oF_1) is a ubiquitous enzyme located in bacterial plasma membranes, mitochondrial inner membranes, and chloroplast thylakoid membranes. It plays a critical role in energy metabolism by synthesizing ATP from ADP and inorganic phosphate (P_i). This enzyme consists of and is separable into two major portions: membrane-embedded F_o and water-soluble F_1. In the simplest version of bacterial F_oF_1 such as F_oF_1s from thermophilic *Bacillus* PS3 and *Escherichia coli*, subunit compositions of F_1 and F_o are, respectively, $\alpha_3\beta_3\gamma\delta\varepsilon$ and ab_2c_{10}. Both portions are rotary motors that share a common rotor shaft $\gamma\varepsilon c_{10}$. Downward proton flow through F_o along the gradient of the electrochemical potential of the proton across the membrane drives the rotation of the c_{10} rotor ring in F_o that drags rotation of the γε rotor shaft of F_1 in the surrounding $\alpha_3\beta_3$ cylinder. This rotation causes cyclic conformational changes in each of the three catalytic β subunits that result in ATP synthesis (1–3).

The isolated F_1, often called F_1-ATPase, catalyzes the ATP hydrolysis reaction that drives the rotation of γε to the direction opposite to that in the ATP synthesis. The minimum subunit composition as an ATPase rotary motor is $\alpha_3\beta_3\gamma$, and we refer to this complex hereinafter as F_1. The γ rotates 120° per net hydrolysis of one ATP. Extensive studies, mainly on F_1 from thermophilic *Bacillus* PS3, have established the nearly complete catalytic scheme of the ATP-driven rotation: Starting from the ATP-waiting state where the orientation angle of the γ is set as 0°, ATP binding to the first β induces the 80°-step rotation of the γ, ADP-release from the second β occurs at some point during this step rotation, and the previously bound ATP in the third β is hydrolyzed at 80°. Then P_i release from either the second or third (not settled) β induces the 40°-step rotation (4–6) to accomplish a single 120° rotation. A recent report indicates that rotation of *E. coli* F_1 is also governed by a scheme similar to that of *Bacillus* F_1 (7).

The torque of this motor has been estimated with various methods (8–13). Among them, an early study that used counter torque reported the torque was ∼50 pN nm/rad (10), indicating that efficiency in chemomechanical energy conversion by F_1 from chemical energy of ATP hydrolysis (ΔG_{ATP}) to mechanical work of rotation reaches almost 100%. A recent study, also using counter torque, revealed that this remarkable efficiency holds in a broad range of ΔG_{ATP} (12). However, the underlying mechanism for this highly efficient energy conversion remains unknown because of an elusive relationship between the catalytic scheme and the energetics. The key question is how the torque varies depending on the γ angle and on ΔG_{ATP}. F_1 is a "stepping motor" driven by discrete chemical events and one might naturally expect that the torque varies depending on the rotary angle by reflecting the catalytic events in the reaction process. Actually, it has been noticed that the torque is not merely constant during rotation. The torque profile along the γ angle in ATP-driven rotation of *E. coli* F_oF_1 showed fluctuation with weak threefold and sixfold symmetries during 360° rotation (10). Also, regular variation of the torque during rotation has been proposed based on the observation that the rotation speed of *E. coli* F_1 is accelerated at three angular regions during 120° rotation (14).

Here we report the torque profiles of *Baccilus* F_1 along the γ angle measured under a quasi-static condition with a conservative force using a single-molecule manipulation system with magnetic tweezers. The obtained torque profiles show a repeat of the steep jump and linear descent approximated by a simple model in which three springs are aligned along a rotary angle of 120°. When

Significance

ATP synthase produces most of the ATP in respiratory and photosynthetic cells. It is a rotary motor enzyme and its catalytic portion F_1-ATPase hydrolyzes ATP to drive rotation of the central γ subunit. Efficiency of chemomechanical energy conversion by this motor is always near-perfect under different ATP hydrolysis energy (ΔG_{ATP}) conditions. However, the mechanism for the efficient conversion remains unknown. We measured the torque as a function of rotation angle under different ΔG_{ATP} conditions and estimated mechanical work. The torque profiles show three sawtooth-like repeats during a single ATP hydrolysis. When concentrations of ATP/ADP and P_i in the environment are changed, the height, and hence the area, of the sawtooth changes accordingly so that mechanical work can always match ΔG_{ATP}.

Author contributions: E.-i.S., K.K., and M.Y. designed research; E.-i.S. performed research; T.S. contributed new reagents/analytic tools; E.-i.S., K.K., and M.Y. analyzed data; and E.-i.S. and M.Y. wrote the paper.

The authors declare no conflict of interest.

This article is a PNAS Direct Submission.

[1]To whom correspondence should be addressed. Email: masasuke.yoshida@cc.kyoto-su.ac.jp.

This article contains supporting information online at www.pnas.org/lookup/suppl/doi:10.1073/pnas.1422885112/-/DCSupplemental.

ΔG_{ATP} changes, the timing of the transition from one spring to the next makes a shift and the area of torque function (mechanical work) changes. The model explains how F_1 always achieves near-perfect chemomechanical energy conversion under various ΔG_{ATP} conditions.

Results

Torque Measured by Single-Molecule Manipulation. F_1 torque was measured using a single-molecule manipulation system composed of magnetic tweezers and magnetic beads (Fig. 1*A*). Magnetic beads under a certain magnetic field behave similarly to springs in their rotational motion on a plane parallel to the magnetic field. The torque on a magnetic bead generated by a magnetic trap (τ_M) can be estimated as shown below (15):

$$\tau_M = \frac{k}{2}\sin 2(\theta_B - \theta_{TC}). \quad [1]$$

In this equation, θ_B, θ_{TC}, and k, respectively, denote rotation angle of the bead, the trap center angle of the magnetic field, and the trap stiffness (for estimates of θ_{TC} and k see *Methods*). To measure the F_1 torque [or $(\theta_B - \theta_{TC})$] at all rotation angles, a magnetic bead attached to F_1 was forcibly rotated at 0.04 Hz in ATP hydrolysis (counterclockwise, defined as a positive angle in this paper) or ATP synthesis (clockwise) direction for six revolutions in the presence of various concentrations of ATP, ADP, and P_i with small k (Fig. S1 *A* and *B*). The relative angular positions of θ_{TC}, θ_B, and γ during magnetic manipulation are schematically illustrated in Fig. 1*B*. During the manipulation in the ATP hydrolysis direction, for example, γ rotates ahead of the controlled magnetic trap (θ_{TC}). The manipulation was sufficiently slow to be assumed as a quasi-static process. Therefore, as far as one θ_{TC} defines one θ_B, the F_1 torque (τ_{F1}) is balanced with τ_M and the magnitudes of the two torques are the same. Fig. 1*C* presents the observed $(\theta_B - \theta_{TC})$ values shown against θ_{TC} when F_1 was forced to rotate to the ATP hydrolysis direction in 10 μM ATP, 10 μM ADP, and 100 μM P_i. At around 1,800–1,900°, the magnetic bead resisted forced rotation; $(\theta_B - \theta_{TC})$ dropped sharply. This occurred because of ADP inhibition, an inhibitory state common to F_1s of many species (16–19). As the forced rotation continued further, F_1 escaped from the inhibited state by the mechanical reactivation as reported (20). The region of ADP inhibition is omitted from analyses hereafter. Two features in Fig. 1*C* are noticeable. First, the magnitude of torque calculated from $(\theta_B - \theta_{TC})$ is ~50 pN nm, on average, throughout six revolutions, consistent with the reported F_1 torque obtained using a conservative force, the same as in this study (10, 12). Second, torque oscillates three times during 120° rotation and each oscillation seems to be composed of a jump, followed by a gradual descent (Fig. 1*D*, black arrowheads). Closer examination reveals that just after the jump, torque often dropped sharply down to the level before the jump and it jumped again (Fig. 1*D*, blue arrowheads). This rapid jump-and-drop behavior suggests that the jump is a transition from one state with a low torque to another state with a high torque, without an intermediate state of significant lifetime, and that these two states are in equilibrium at angles near the transition point. Thus, the F_1 motor is activated three times during hydrolysis of one ATP. As expected from a quasi-static manipulation, similar oscillation was observed when F_1 was forced to rotate to the ATP synthesis direction (Fig. S1 *C* and *D*).

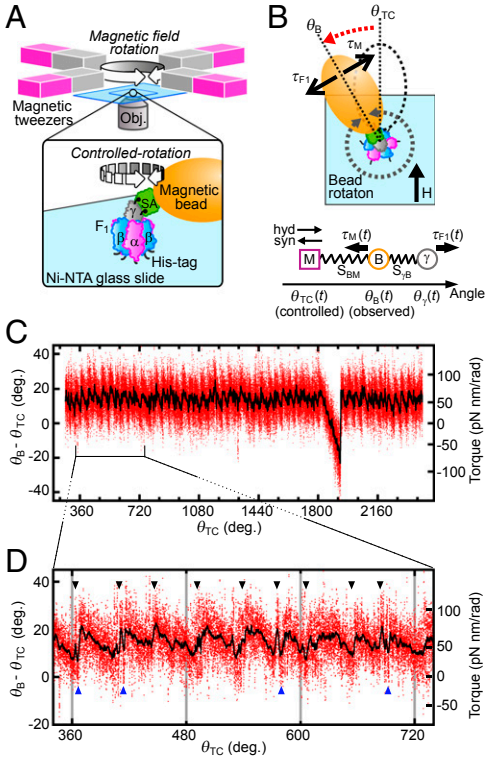

Fig. 1. Oscillation of F_1 torque probed using magnetic tweezers. (*A*) Experimental design (not to scale). Rotation of magnetic beads attached to F_1 is manipulated with magnetic tweezers. (*B*) (*Upper*) Angular displacement of trapped beads in the presence of F_1 torque. θ_{TC} indicates an angular position at which magnetic beads are trapped under a certain magnetic field in the absence of F_1 torque (τ_{F1}). In the presence of τ_{F1}, the bead angle shifts to θ_B so that τ_{F1} and magnetic torque (τ_M) are balanced. (*Lower*) Positional relationship between γ, bead, and magnetic trap center at time t during manipulation. $S_{\gamma B}$ represents external elastic component that cause the shift of θ_B from θ_γ (for the definition and estimation see *Methods*, *Torque Profile As a Function of* θ_γ). S_{BM} is the putative spring by magnetic trap. Its magnitude of torque is defined with Eq. **1**. (*C*) Example trace of F_1 torque as a function of θ_{TC}. Raw data points during controlled rotation (0.04 Hz, ATP hydrolysis direction) are shown in red. Black shows a result of 200-point median filtering. The substrate concentrations are 10 μM (ATP), 10 μM (ADP), and 100 μM (P_i) (condition *i* in Fig. 2*C*). (*D*) Magnified plot. Torque jumps are indicated by arrowheads.

Efficiency of Chemomechanical Energy Conversion. To analyze the jump-and-descent pattern, data were replotted against θ_B because the torque measured at the angle of θ_{TC} represents the torque produced by F_1 at the angle of θ_B. Then, whole torque plots except the region of ADP inhibition were superimposed into a 360° unit and filtered by density of data points (for analysis details, see *SI Text* and Fig. S2; excluding ADP inhibition, see Fig. S3). Because the timing of jumps statistically fluctuated, simple averaging of superimposed data of the jump areas would produce a torque profile with continuous increase of torque and make the jump ambiguous. Density filtering, on the contrary, differentiates the regions of clusters of data points, where the torque changed gradually (Fig. 2*A*, colored regions), and the regions of relatively scarce data points between clusters, where the torque changed steeply. Each cluster was running-averaged (Fig. 2*A*, bold black lines) and the adjacent average lines were connected at the angular position where the point density of the preceding cluster became equal to that of the next cluster (Fig. 2*A*, broken black lines). The shape of the connecting line was not obtained from experiments and we simply assumed a straight line. The resultant sawtooth-like torque profile well reproduces the regular jump-and-descent pattern of the torque (Fig. S4). The mechanical work (torque × traveled angle) is defined by the area of the torque-angle plot and the area from 0° to 360° (shaded area) in Fig. 2*B* represents the mechanical work done by F_1 against the magnetic trap during 360° revolution. We measured torque profiles under seven conditions (denoted as *i* to *vii* hereafter), in which concentrations of ATP, ADP, and P_i differed 100 times (Fig. 2*C*, *Upper*), and estimated the amounts of mechanical work of F_1 during 360° revolution.

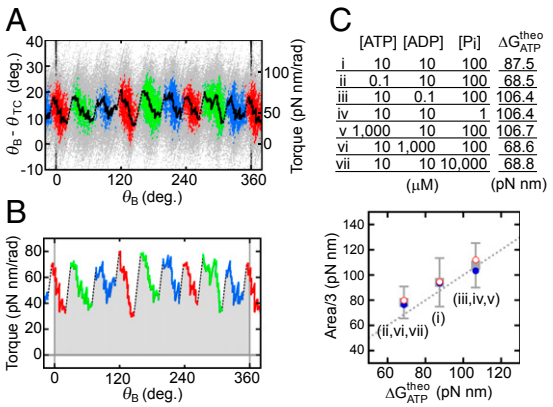

Fig. 2. Three states of F_1 and the efficiency of chemomechanical energy conversion. (*A*) Clustering into three states. Raw data points of angular deviation during six revolutions are superimposed using a 360° unit (gray points). Data points are selected by their density with a threshold value and are clustered into states of three kinds, for a total of nine states (red, green, and blue clusters; *SI Text*). Bold black lines show running averages of respective clusters. (*B*) Torque profile and mechanical work. The lines in *A* are reported in torque versus θ_B. Shaded areas give mechanical work done by F_1. (*C*) Efficiency of chemomechanical energy conversion. (*Upper*) A list of substrate conditions and calculated free energy change of ATP hydrolysis (ΔG_{ATP}) (21). (*Lower*) Comparison of observed mechanical works per 120° rotation obtained from *B* with ΔG_{ATP} (gray squares). Error bars represent SDs. Average mechanical work in ATP hydrolysis and ATP synthesis are shown respectively in blue filled circles and red open circles. The dotted line represents 100% chemomechanical energy conversion.

One-third of the estimated work, which corresponds to the work during hydrolysis of a single ATP molecule, is shown against the calculated free energy change accompanied with hydrolysis of a single ATP molecule (21) (ΔG_{ATP}). Results show that *ii*, *vi*, and *vii* gave almost equal work, as expected from their same magnitude of ΔG_{ATP}; such was also the case for *iii*, *iv*, and *v* (Fig. S5). The average work for *ii*, *vi*, and *vii* and that for *iii*, *iv*, and *v*, as well as the work for *i*, is close to the values of ΔG_{ATP} under the corresponding substrate concentrations (Fig. 2*C*, *Lower*). The works during ATP synthesis were also estimated from the forced rotation of the same F_1 molecules to the ATP synthesis direction. As seen, in the same substrate concentrations, the work during ATP synthesis was very similar to the work during ATP hydrolysis. These results are expected from the quasi-static manipulation during rotations, either to the ATP hydrolysis or to the synthesis direction, and confirm the high efficiency close to 100% in chemomechanical energy conversion by F_1 not only for ATP hydrolysis but also for ATP synthesis in a broad range of ΔG_{ATP}. This result also implies that the ATP synthesis reaction is coupled tightly to the mechanical rotation forced by magnetic tweezers at low speed, which is consistent with previously reported results (22).

Torque Profiles in Different ΔG_{ATP} Conditions. To understand how F_1 achieves near-perfect chemomechanical energy conversion under various ΔG_{ATP} conditions, the torque profiles in conditions *ii*–*vii* were compared with the profile in condition *i*. All torque profiles of rotation to the ATP hydrolysis direction in condition *i* (and *ii*–*vii*) obtained from three independent experiments using different F_1 molecules were sectioned into 120° rotation, superimposed, and averaged to obtain the most probable profiles of the torque (Fig. S6, for detailed procedures see *SI Text*, *Torque Profiles of Each Condition*). Fig. 3 *A*–*C* show responses of the torque profiles to 100-fold or 1/100-fold increase/decrease of [ATP], [ADP], or [P_i] from condition *i*. We note that each torque profile shown here is an average of both profiles of ATP hydrolysis and ATP synthesis reactions, because these two profiles of both reactions are almost identical in each condition (Fig. S7*A*). Fig. 3 *A*–*C* directly capture the mechanism whereby this motor adapts its work according to an environmental change of ΔG_{ATP}. First, the location and slope of the descending portions after the transitions in torque profiles were changed little or not changed at all. Indeed, when the torque profiles of all 14 conditions (7 substrate conditions × 2 directions of reaction) are superimposed, the descending portions overlap well and make three bundles of lines irrespective of direction of rotation and transition timings (Fig. S7*B*). Thus, properties of each of the three states, depicted as I, II and III, are unaffected by ΔG_{ATP}. Second, timings of transitions shift when ΔG_{ATP} changed. When [ATP] was changed, only the transition III–I among three transitions made a significant shift to early (100-fold ATP) or late (1/100-fold ATP) timing (Fig. 3*A*). This shift causes the change of the mechanical work (ΔW) defined by the change of the area as illustrated (Fig. 3*D*). Even though resolution of the measurements limits the fine quantitative analysis, the ΔW produced by the timing shift of transition III–I can explain most (~75%, 1/100-fold ATP) or a significant part (~40%, 100-fold ATP) of the changed amount of ΔG_{ATP} ($\Delta\Delta G_{ATP} = \sim\pm 19$ pN nm). Also, when [ADP] was changed (Fig. 3*B*), the transition III–I occurred early (1/100-fold ADP) or late (100-fold ADP), although a small timing shift was also observed in the transition II–III. The ΔW at transition III–I is ~45% (1/100-fold ADP) or 35% (100-fold ADP) of the $\Delta\Delta G_{ATP}$. In the case of P_i (Fig. 3*C*), a 100-fold increase in [P_i] results in the delay of transition II–III that accompanies ΔW corresponding to ~45% of $\Delta\Delta G_{ATP}$. No major shift was observed when [P_i] was diluted to 1/100-fold, probably because the concentration of P_i (1 μM) in this experiment was too low for quantitative analysis, that is, two to three orders lower than the Michaelis–Menten constant of P_i (0.55 mM) (23), and other anion could compete for the same site with P_i. Contrary to other

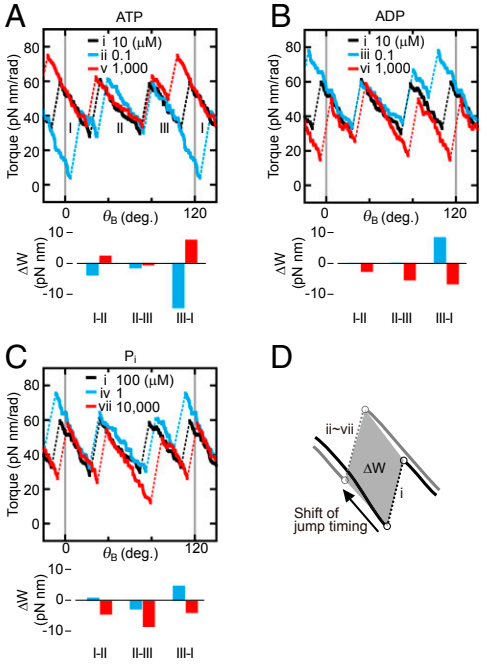

Fig. 3. Torque profiles in the presence of different concentrations of (*A*) ATP, (*B*) ADP, and (*C*) P_i. Black lines are the torque profile of condition *i* (ATP = 10 μM, ADP = 10 μM, and P_i = 100 μM). Blue and red lines represent the torque profiles in 100-fold and 1/100-fold concentration of the indicated substrate, respectively. The areas sandwiched between torque profile of condition *i* and those of conditions *ii*–*vii* during the transition are obtained as illustrated in *D*. The areas are converted to the variations of the mechanical work (ΔW) generated from the shift of the transition timing and shown below each panel.

transitions, the transition timings between state I and state II are affected only slightly by the concentration changes of the substrates. It has been shown that the angular position of ATP binding, ADP release, and P_i release are around 0°, 0° (or somewhere between 0° and 80°), and 80°, respectively (4, 6, 24). Taking into account this rotation scheme, it seems that the transition between state III and state I is caused by binding/release of ATP/ADP and the transition between state II to state III is governed by P_i release/binding.

Torque Profile of F_1 Without ATP Hydrolysis. To understand the torque profile of F_1 without ATP hydrolysis, the buffer in the observation chamber containing ATP, ADP, and P_i in which F_1 showed a typical jump-and-descent pattern (Fig. 4*A*) was exchanged to the buffers lacking ATP, and the torque profile was obtained for the same F_1 molecule from the forced rotation of the bead to the ATP hydrolysis direction (Fig. 4*B*). In ADP and P_i, the torque is negative at the γ angle 0°, but it jumps to ∼30 pN nm at about 40°, which is followed by a gradual decrease to ∼−40 pN nm in a 120° rotation. It is noteworthy that the jump occurs at the same position (about 40°) as the transition jumps from state I to state II in the presence of ATP. Without ATP hydrolysis, the net amount of the work done by F_1 during 120° rotation is expected to be zero; indeed, the work calculated from the torque profiles is −2.7 pN nm, which is virtually zero. The energy supplied from the magnetic trap in the negative torque region is stored as the energy of elastic strain in the protein conformation and it is released during positive torque regions. A similar torque profile was observed in the buffer containing ADP (Fig. 4*C*). In the buffer containing only P_i and in the buffer containing no ATP, ADP, and P_i, a jump at about 40° was also observed, although its magnitude was small (Fig. 4 *D* and *E*). Consequently, without net catalysis, F_1 has an intrinsic rotary potential such that it exerts a torque jump at around 40°. It is tempting to infer that the transition from state I to state II observed in the presence of ATP is attributable to this intrinsic property of F_1 (Fig. 4*F*), although a possibility remains that this property changes during catalysis.

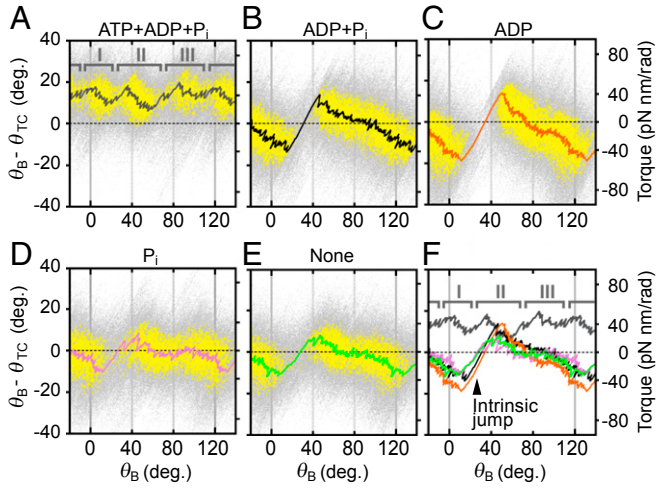

Fig. 4. Intrinsic torque jump of F_1. Data points of angular displacement ($\theta_B - \theta_{TC}$) obtained from controlled rotation to the ATP hydrolysis direction (0.04 Hz, six revolutions) are shown in 120° unit (gray points), and filtered by its density (yellow points) these are almost same procedures as steps 1–3 in Fig. S2. The extracted dense points are median-filtered with 500 points without clustering process (black line): (*A*) ATP, ADP, and P_i = 10, 10, and 100 μM (condition *i*); (*B*) 0, 10, and 100 μM; (*C*) 0, 10, and 0 μM; (*D*) 0, 0, and 100 μM; and (*E*) no substrate. The change of substrate was achieved by exchange of the solution in the observation chamber. These data were obtained from one of three F_1 molecules used in the torque quantification of this research. (*F*) Intrinsic torque jump and transition between states I and II. Torque traces in *A*–*E* were overlaid.

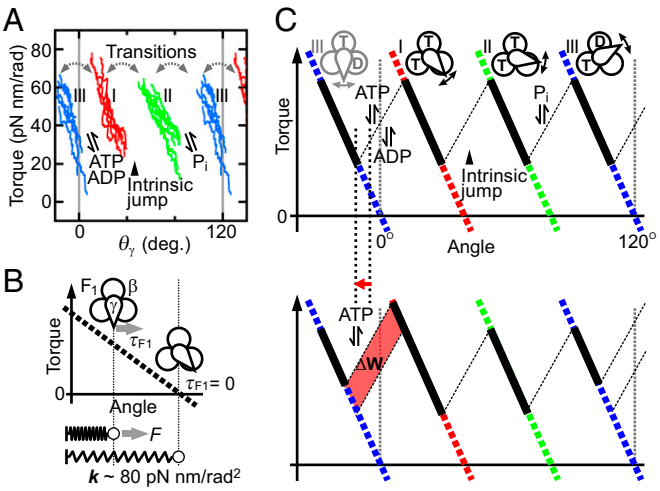

Fig. 5. Tandem spring model of F_1 rotation. (*A*) Rotation with three state transitions. Torque traces as a function of angular position of γ subunit (θ_γ) obtained from all conditions tested in this study are superimposed (*SI Text*). (*B*) Approximation of a certain state of F_1 as a spring. (*C*) Tandem spring model of F_1 rotation. States I, II, and III are approximated as springs. F_1 generates torque continuously by the transitions of these three springs. Transition between states I and II is triggered by intrinsic property of F_1. When [ATP] increases, the transition position from state III to I shifts to the left, which results in the increase of mechanical work of F_1 (red area). T and D represent ATP and ADP, respectively.

Discussion

This study yielded torque profiles of F_1 during rotation from displacement angles of the attached magnetic bead from the angles of external magnetic field. The observed bead angle might deviate from the true angle of the γ subunit because of external elastic components such as histidine tags, linkers between γ and streptavidin, and so on (Fig. 1*B*). We estimated the stiffness of external elastic components in each F_1 molecule (see *Methods*, *Torque Profile As a Function of* θ_γ) and deduced the torque profile as a function of the γ angle (Fig. 5*A* and Fig. S8). However, the correction did not alter three jump-and-descent features of the profiles. Interestingly, in the corrected plot, there is no overlap along θ_γ between three states. This means that the γ angle is the only determinant of the states, at least under the conditions we tested in this study. This would be advantageous for avoiding uncoupled rotation because the γ angle corresponds one-to-one with the F_1 state.

The presence of three jump-and-descent patterns of torque in a 120° rotation indicates that the F_1 motor is activated three times by a net hydrolysis of one ATP. In other words, F_1 undergoes transitions between three different states during catalysis. Setting the γ angular position where F_1 binds ATP as 0°, the transitions occur at around 0°, 40°, and 80°. According to the established catalytic scheme of bacterial F_1, binding of ATP to F_1 induces the stepping rotation of the γ from 0° to 80° and release of P_i from F_1 does so from 80° to 120° (4–6). Similar stepwise rotation of the γ subunit was simulated for bovine F_1 (25, 26). Therefore, state III defined in this study corresponds to F_1 in the state waiting for ATP binding (pre-ATP-binding state) and state II corresponds to F_1 in the state waiting for P_i release (pre-P_i-release state). ATP binding to the former and P_i release from the latter induce the transition III–I and the transition II–III, respectively.

The transition between state I and state II at around 40° is affected little by concentrations of substrates and therefore does not

accompany binding/release of substrates. Because a similar transition was observed even in the absence of all substrates, the transition I–II can be some conformational rearrangement induced automatically at around 40°. Then, it seems that, when the γ in F_1 in state I reaches the point beyond 40° during a step rotation from 0° to 80°, a conformational rearrangement takes place in F_1 generating state II that is capable of exerting a high torque. Energetically, a fraction of energy gained by ATP binding at 0° is stored in F_1 as conformational strain and is used for driving a conformational rearrangement at 40°. Interestingly, molecular dynamics simulation of F_1 predicts that a 80°-step rotation after ATP binding is driven by a relaying pattern of torques, that is, the torque generated primarily on the N-terminal helix region of the γ is reduced as the γ rotates and is taken over at around 40° by the torque generated primarily on C-terminal helix region of the γ (27). We have observed pauses of rotation at 0° at low [ATP] and at 80° at high [P_i] but not at 40° under any conditions tested. The 40° pause would become apparent when the transition I–II is delayed. However, the transition I–II takes place automatically when the γ reaches 40° and there is no means, so far, to make the transition slow. Recently, it was found that human F_1 makes three pauses in a 120° rotation (28). However, a start of step rotation from each pause is induced by a distinct chemical event in catalysis and may not directly correspond to the transition I–II that is intrinsic.

In each of the three states, torque decreases almost linearly with the angle (Fig. 5*A*), enabling approximation of each state as a simple spring (Fig. 5*B*), even though many interactions of γ with the $\alpha_3\beta_3$ cylinder might be involved in torque generation. In Fig. 5*C* we present a simple model of F_1 rotation by treating these springs as the minimum constituents for torque generation. In this model, F_1 generates torque continuously by transitions between these three springs with similar spring constants (~80 pN nm/rad^2). This value is far from the center value but within a possible range of the previously reported value (223 ± 141 pN nm/rad^2) (29). The first spring (transition III–I) is energized by ATP binding, the second (transition I–II) by the intrinsic rotary property of F_1, and the third (transition II–III) by P_i release. This model provides a simple physical view of how the chemical cycle is coupled with torque generation.

The chemomechanical energy conversion efficiency of F_1 is close to 100% under various ΔG_{ATP} conditions (12). The torque profile found here explains how F_1 achieves this remarkable task. Fig. 5*C* illustrates how F_1 responds to the increase of [ATP] and adjusts its mechanical work accordingly. The equilibrium constants for nucleotide bindings/dissociations are functions of the γ angle (30–33). Therefore, as [ATP] is increased, the angular position of binding/dissociation of ATP shifts to the left (Fig. 5*C*, red arrow) at the point where the spring is shorter. The shorter the spring becomes, the greater the force to extend becomes because of the nature of a spring (Fig. 5*B*). This shift invariably increases the area of the sawtooth, that is, the mechanical work. This study shows that the following two properties of the torque profile of the F_1 motor ensure ~100% energy conversion under various ΔG_{ATP} conditions: (*i*) shift of the angular positions of binding/dissociation of substrates according to their concentrations and (*ii*) changing its force (torque) according to the angular position of substrate binding/dissociation, which is readily accomplished by a simple spring.

Besides the main conclusion described above, this study gives implications for two issues. This study unveils the torque function of F_1 in the absence of ATP for the first time, to our knowledge (Fig. 4 *B*–*E*). Without ATP, regardless of the presence or absence of ADP and P_i, the torque is zero at γ angles of around 30° and around 80°. However, the γ cannot stay at 30° because it moves away in either direction when the torque fluctuates thermally. In contrast, the γ can stay at 80° because the fluctuating γ is always pulled back to the 80° position. Then, note that 80° is the only stable position in 120° for the γ to stay in the resting F_1 molecule that is not carrying out catalysis. This explains why the majority of crystal structures reflect a state of the enzyme with the angular position of the γ ~80°, which is around the position where hydrolysis of ATP occurs in one of the catalytic sites (34–36). This study also reveals that torque of F_1 jumps at every ~40°, but not at 80°–40° intervals as thought previously. It is supposed that when F_oF_1 rotates by proton flow through the c_{10} rotor ring in F_o, torque should be produced 10 times in one revolution, that is, at every 36°. Then, the elastic components in the rotor shaft and peripheral stalk could buffer this small angle difference more easily than thought before, and ensure smooth, tight coupling between F_1 and F_o (10, 37–39). Comparable stiffness of the rotation-driving springs of F_1 (~80 pN nm/rad^2) to the reported stiffness of the rotor shaft (~68 pN nm/rad^2) (38) might further contribute to the smooth, tight coupling.

Methods

Microscopy. Rotation of magnetic beads was imaged on an inverted microscope (IX70; Olympus Corp.) with a stable mechanical stage. The bright-field image of magnetic beads, illuminated by a mercury lamp (HBO 103W/2; Osram GmbH), was captured alternately with two CCD cameras. First, for the selection of molecules to be observed, stepping rotation of F_1 at 100 nM ATP was captured with a CCD camera (CCD-300-RC; Dage-MTI) at the video rate of 30 frames per second. The centroid motion of beads was analyzed using software (Celery; library) on a computer in real time, enabling us to check the degree of centrosymmetry, stability of the orbit, and the three ATP waiting positions of beads before, during, and after the several forcible rotations applied by magnetic tweezers. Next, for torque measurements, the bead image was captured with another CCD camera (ICL-B0620M-KC; Imperx) at the video rate of 1,000 frames per second and recorded on another computer using acquisition software (XCAP; Epix).

Magnetic tweezers consisted of two opposing pairs of electromagnets. They were positioned ~10 mm above the microscope stage (15) (Fig. 1*A*). The magnetic field direction and strength were controlled by changing the electric voltage applied to the pairs of electromagnets, which was done with software (Celery; library). Magnetic beads were rotated in both directions at 0.04 Hz with the 45–57 Gauss magnetic field at the sample position.

To ascertain the moment of the start and the finish of the magnetic manipulations, a shutter (Uniblitz VS14; Vincent Associates) was placed between the mercury lamp and condenser lens, which closed only at the moment of the start and the finish of each magnetic manipulation. The shutter operations were confirmed by the intensity changes of the bright-field image. The typical duration of the closed state of each shutter operation was ~10 ms.

Estimation of Trap Stiffness and the Trap Center Angle. Thermal fluctuation of beads in the absence of magnetic field was recorded for ~30 s (~30,000 frames) for the F_1 molecule in an MgADP inhibited state (Fig. S9*A*, black). Next, we applied a magnetic field with the same magnitude for the torque measurement experiments at a certain angle at which the bead angle did not make a shift from the inhibited position, and fluctuation of the beads was recorded again for ~30 s (Fig. S9*A*, red). The histogram of the angular distribution of beads in the presence of the magnetic trap was divided by that in the absence of the magnetic trap for each bin (Fig. S9*B*). Average square roots of variances of the distributions are 12.0° (in the absence of magnetic field) and 6.6° (in the presence of magnetic field). The obtained histogram was normalized by area. The resultant histogram was assumed to reflect only the potential formed by the magnetic trap. It was fitted with a Gaussian probability density function based on the linear approximation of magnetic torque (Eq. **1**), $\tau_M \sim k(\theta - \theta_{TC})$, which holds at small $(\theta - \theta_{TC})$:

$$P(\theta) = (2\pi\sigma^2)^{-\frac{1}{2}} \cdot \exp\left(-\frac{(\theta-\theta_{TC})^2}{2\sigma^2}\right). \quad [2]$$

Here, θ stands for the bead angle in radians, θ_{TC} denotes the trap center angle, and σ^2 represents the variance. The trap stiffness (k) is given as $k = k_BT\sigma^{-2} \sim 4.1\sigma^{-2}$ (pN nm/rad^2), where k_B is Boltzmann's constant and T is the absolute temperature. These measurements were performed in 0.1 μM ATP + 10 μM ADP + 100 μM P_i (condition *ii*) or in 10 μM ATP + 1,000 μM ADP + 10 μM P_i (condition *vi*) to allow F_1 to lapse easily into MgADP inhibition, which can occur at three angular positions in 360°. The same measurement was

performed at all three positions for each molecule. Values of the trap stiffness of three F_1 molecules used for experiments were 175.6 ± 9.3 pN nm/rad^2, 241.0 ± 13.9 pN nm/rad^2, and 245.6 ± 24.5 pN nm/rad^2 (mean ± SD).

The external magnetic field was rotated at 0.04 Hz to the direction of either ATP hydrolysis or ATP synthesis and θ_{TC} at time t was given as $\theta_{TC}(t) = \theta_{TC}(0) + 2\pi{\cdot}0.04{\cdot}t$ (ATP hydrolysis direction) or as $\theta_{TC}(t) = \theta_{TC}(0) - 2\pi{\cdot}0.04{\cdot}t$ (ATP synthesis direction).

Torque Profile As a Function of θ_γ. Bead angle is the only observable object in this system. However, the bead angle deviated from the actual angle of γ relative to $\alpha_3\beta_3$ at the stator orifice owing to the external elastic components such as histidine tags, $\alpha_3\beta_3$ ring, globular portion of γ, linkers between γ and streptavidin, and streptavidin itself (Fig. 1*B*). External stiffness (k_{ex}) defined by these components, that is, spring constant of $S_{\gamma B}$, was assumed as below for each molecule. Okuno et al. (29) have reported that the spring constant of γ motion at the stator orifice in the ATP waiting state (internal stiffness, k_{in}) was 223 pN nm/rad^2. Observable angular fluctuation of bead in ATP waiting state is determined by total stiffness $(k_{total} = 1/(k_{in}^{-1} + k_{ex}^{-1}))$ composed of internal and external stiffness. To determine k_{total}, we observed bead motion in the ATP waiting state under 100 nM ATP for each molecule. According to the variance (σ^2) of Gaussian probability density functions (Eq. **2**) fitted to the obtained angular distributions of bead, we determined k_{total} for each molecule as 56.4, 111.8, and 165.2 pN nm/rad^2 ($k_{total} = k_BT\sigma^{-2} \sim 4.1\sigma^{-2}$). Finally, based on these values, we could assume $k_{ex}(k_{ex} = 1/(k_{total}^{-1} - k_{in}^{-1}))$ for each molecule as 75.4, 224.0, and 637.8 pN nm/rad^2. Then, we estimate average lines of torque as a function of θ_γ from that of θ_B by a correction equation for each molecules: $\theta_\gamma = \theta_B + \tau(\theta_B)/k_{ex}$. The torque profiles as the function of θ_γ were derived from the obtained average lines as a function of θ_γ with same procedures described in *SI Text, Torque Profiles of Each Condition*. In Fig. S8 we overlay the corrected torque profiles of all seven conditions (black lines).

ACKNOWLEDGMENTS. We thank all members of our laboratory for technical support and discussion. We also thank Ryota Iino (University of Tokyo) for critical discussion and Rikiya Watanabe (University of Tokyo) for construction of the magnetic tweezers system. This work was partly supported by Japan Society for the Promotion of Science Grant-in-Aid for Scientific Research 90049073 (to M.Y.) and the Ministry of Education, Culture, Sports, Science, and Technology-supported Program for the Strategic Research Foundation at Private Universities, 2011–2016.

1. Boyer PD (1993) The binding change mechanism for ATP synthase—some probabilities and possibilities. *Biochim Biophys Acta* 1140(3):215–250.
2. Diez M, et al. (2004) Proton-powered subunit rotation in single membrane-bound F_oF_1-ATP synthase. *Nat Struct Mol Biol* 11(2):135–141.
3. Yoshida M, Muneyuki E, Hisabori T (2001) ATP synthase—a marvellous rotary engine of the cell. *Nat Rev Mol Cell Biol* 2(9):669–677.
4. Adachi K, et al. (2007) Coupling of rotation and catalysis in F_1-ATPase revealed by single-molecule imaging and manipulation. *Cell* 130(2):309–321.
5. Watanabe R, Iino R, Noji H (2010) Phosphate release in F_1-ATPase catalytic cycle follows ADP release. *Nat Chem Biol* 6(11):814–820.
6. Yasuda R, Noji H, Yoshida M, Kinosita K, Jr, Itoh H (2001) Resolution of distinct rotational substeps by submillisecond kinetic analysis of F_1-ATPase. *Nature* 410(6831):898–904.
7. Bilyard T, et al. (2013) High-resolution single-molecule characterization of the enzymatic states in Escherichia coli F_1-ATPase. *Philos Trans R Soc Lond B Biol Sci* 368(1611):20120023.
8. Hayashi K, Ueno H, Iino R, Noji H (2010) Fluctuation theorem applied to F_1-ATPase. *Phys Rev Lett* 104(21):218103.
9. Noji H, Yasuda R, Yoshida M, Kinosita K, Jr (1997) Direct observation of the rotation of F_1-ATPase. *Nature* 386(6622):299–302.
10. Pänke O, Cherepanov DA, Gumbiowski K, Engelbrecht S, Junge W (2001) Viscoelastic dynamics of actin filaments coupled to rotary F-ATPase: Angular torque profile of the enzyme. *Biophys J* 81(3):1220–1233.
11. Spetzler D, et al. (2006) Microsecond time scale rotation measurements of single F_1-ATPase molecules. *Biochemistry* 45(10):3117–3124.
12. Toyabe S, Watanabe-Nakayama T, Okamoto T, Kudo S, Muneyuki E (2011) Thermodynamic efficiency and mechanochemical coupling of F_1-ATPase. *Proc Natl Acad Sci USA* 108(44):17951–17956.
13. Yasuda R, Noji H, Kinosita K, Jr, Yoshida M (1998) F_1-ATPase is a highly efficient molecular motor that rotates with discrete 120 degree steps. *Cell* 93(7):1117–1124.
14. Martin JL, Ishmukhametov R, Hornung T, Ahmad Z, Frasch WD (2014) Anatomy of F_1-ATPase powered rotation. *Proc Natl Acad Sci USA* 111(10):3715–3720.
15. Saita E, et al. (2010) Activation and stiffness of the inhibited states of F_1-ATPase probed by single-molecule manipulation. *J Biol Chem* 285(15):11411–11417.
16. Carmeli C, Lifshitz Y (1972) Effects of P_i and ADP on ATPase activity in chloroplasts. *Biochim Biophys Acta* 267(1):86–95.
17. Drobinskaya IY, Kozlov IA, Murataliev MB, Vulfson EN (1985) Tightly bound adenosine diphosphate, which inhibits the activity of mitochondrial F_1-ATPase, is located at the catalytic site of the enzyme. *FEBS Lett* 182(2):419–424.
18. Dunham KR, Selman BR (1981) Interactions of inorganic phosphate with spinach coupling factor 1. Effects on ATPase and ADP binding activities. *J Biol Chem* 256(19):10044–10049.
19. Feniouk BA, Suzuki T, Yoshida M (2007) Regulatory interplay between proton motive force, ADP, phosphate, and subunit epsilon in bacterial ATP synthase. *J Biol Chem* 282(1):764–772.
20. Hirono-Hara Y, Ishizuka K, Kinosita K, Jr, Yoshida M, Noji H (2005) Activation of pausing F_1 motor by external force. *Proc Natl Acad Sci USA* 102(12):4288–4293.
21. Krab K, van Wezel J (1992) Improved derivation of phosphate potentials at different temperatures. *Biochim Biophys Acta* 1098(2):172–176.
22. Itoh H, et al. (2004) Mechanically driven ATP synthesis by F_1-ATPase. *Nature* 427(6973):465–468.
23. Soga N, Kinosita K, Jr, Yoshida M, Suzuki T (2011) Efficient ATP synthesis by thermophilic Bacillus F_oF_1-ATP synthase. *FEBS J* 278(15):2647–2654.
24. Watanabe R, Iino R, Shimabukuro K, Yoshida M, Noji H (2008) Temperature-sensitive reaction intermediate of F_1-ATPase. *EMBO Rep* 9(1):84–90.
25. Nam K, Pu J, Karplus M (2014) Trapping the ATP binding state leads to a detailed understanding of the F_1-ATPase mechanism. *Proc Natl Acad Sci USA* 111(50):17851–17856.
26. Okazaki K, Hummer G (2013) Phosphate release coupled to rotary motion of F_1-ATPase. *Proc Natl Acad Sci USA* 110(41):16468–16473.
27. Pu J, Karplus M (2008) How subunit coupling produces the gamma-subunit rotary motion in F_1-ATPase. *Proc Natl Acad Sci USA* 105(4):1192–1197.
28. Suzuki T, Tanaka K, Wakabayashi C, Saita E, Yoshida M (2014) Chemomechanical coupling of human mitochondrial F_1-ATPase motor. *Nat Chem Biol* 10(11):930–936.
29. Okuno D, Iino R, Noji H (2010) Stiffness of gamma subunit of F_1-ATPase. *Eur Biophys J* 39(12):1589–1596.
30. Adachi K, Oiwa K, Yoshida M, Nishizaka T, Kinosita K, Jr (2012) Controlled rotation of the F_1-ATPase reveals differential and continuous binding changes for ATP synthesis. *Nat Commun* 3:1022.
31. Kinosita K, Jr, Adachi K, Itoh H (2004) Rotation of F_1-ATPase: How an ATP-driven molecular machine may work. *Annu Rev Biophys Biomol Struct* 33:245–268.
32. Watanabe R, et al. (2012) Mechanical modulation of catalytic power on F_1-ATPase. *Nat Chem Biol* 8(1):86–92.
33. Iko Y, Tabata KV, Sakakihara S, Nakashima T, Noji H (2009) Acceleration of the ATP-binding rate of F_1-ATPase by forcible forward rotation. *FEBS Lett* 583(19):3187–3191.
34. Masaike T, Koyama-Horibe F, Oiwa K, Yoshida M, Nishizaka T (2008) Cooperative three-step motions in catalytic subunits of F_1-ATPase correlate with 80 degrees and 40 degrees substep rotations. *Nat Struct Mol Biol* 15(12):1326–1333.
35. Okuno D, et al. (2008) Correlation between the conformational states of F_1-ATPase as determined from its crystal structure and single-molecule rotation. *Proc Natl Acad Sci USA* 105(52):20722–20727.
36. Sielaff H, Rennekamp H, Engelbrecht S, Junge W (2008) Functional halt positions of rotary F_oF_1-ATPase correlated with crystal structures. *Biophys J* 95(10):4979–4987.
37. Junge W, Sielaff H, Engelbrecht S (2009) Torque generation and elastic power transmission in the rotary F_oF_1-ATPase. *Nature* 459(7245):364–370.
38. Sielaff H, et al. (2008) Domain compliance and elastic power transmission in rotary F_oF_1-ATPase. *Proc Natl Acad Sci USA* 105(46):17760–17765.
39. Czub J, Grubmüller H (2011) Torsional elasticity and energetics of F_1-ATPase. *Proc Natl Acad Sci USA* 108(18):7408–7413.
40. Hirono-Hara Y, et al. (2001) Pause and rotation of $F(_1)$-ATPase during catalysis. *Proc Natl Acad Sci USA* 98(24):13649–13654.